ACS SENSORS

Article

Cite This: ACS Sens. XXXX, XXX, XXX−XXX

pubs.acs.org/acssensors

Pathogenic Bacteria Detection Using RNA-Based Loop-Mediated Isothermal-Amplification-Assisted Nucleic Acid Amplification via Droplet Microfluidics

Morteza Azizi,[†] Meisam Zaferani,[†] Soon Hon Cheong,[‡] and Alireza Abbaspourrad*[,†]

[†]Department of Food Science, College of Agricultural and Life Sciences, Cornell University, Ithaca, New York 14853, United States

[‡]Department of Clinical Sciences, College of Veterinary Medicine, Cornell University, Ithaca, New York 14853, United States

Supporting Information

ABSTRACT: Nucleic acid amplifications, such as polymerase chain reaction (PCR), are very beneficial for diagnostic applications, especially in the context of bacterial or viral outbreaks due to their high specificity and sensitivity. However, the need for bulky instrumentation and complicated protocols makes these methods expensive and slow, particularly for low numbers of RNA or DNA templates. In addition, implementing conventional nucleic acid amplification in a high-throughput manner is both reagent- and time-consuming. We bring droplet-based microfluidics and loop-mediated isothermal amplification (LAMP) together in an optimized operational condition to provide a sensitive biosensor for amplifying extracted RNA templates for the detection of *Salmonella typhimurium* (targeting the *invA* gene). By simultaneously performing ∼10^6 LAMP-assisted amplification reactions in picoliter-sized droplets and applying a new mathematical model for the number of droplets necessary to screen for the first positive droplet, we study the detection limit of our platform with pure culture and real samples (bacterial contaminated milk samples). Our LAMP-assisted droplet-based microfluidic technique was simple in operation, sensitive, specific, and rapid for the detection of pathogenic bacteria *Salmonella typhimurium* in comparison with well-established conventional methods. More importantly, the high-throughput nature of this technique makes it suitable for many applications in biological assays.

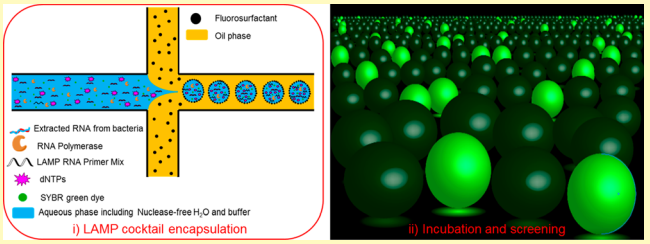

KEYWORDS: *pathogenic bacteria detection, LAMP, droplet microfluidics, biosensor, nucleic acid amplification*

Pathogens lead to serious infectious diseases worldwide and cause enormous economic losses, making the detection of pathogenic bacteria essential to public health.[1−5] Particularly, *Salmonella* serotypes are involved in a wide variety of human and animal diseases, and their pathogenicity is mainly due to genetic characteristics mediating virulence, invasive capacity, immune invasion, and antibiotic resistance.[5−7] The global human health impact of *Salmonella typhimurium* (*S. typhimurium*) is high, estimated to cause 93.8 million human infections (80.3 million of which are foodborne) and 155,000 deaths annually worldwide.[1,6,8]

Polymerase chain reaction (PCR) is the current gold standard of nucleic acid amplification (NAA), especially in diagnostics and point-of-care platforms.[9,10] However, there are two big concerns: (i) it requires bulky and expensive instruments for temperature cycling, which can be a significant challenge in resource-limited countries.[11] Moreover, the turnaround time for a low number of extracted nucleic acid templates is often too long for critical applications, including dangerous bacterial or viral outbreaks. (ii) It can be expensive to prepare the PCR reaction mixture to run parallel experiments in a high-throughput mode using conventional approaches.[11]

To address the first shortcoming, several isothermal NAA methods such as strand displacement amplification,[12] helicase-dependent amplification,[13] nicking enzyme amplification reaction,[14] and loop-mediated isothermal amplification (LAMP)[15,16] have recently been developed for resource-limited conditions. LAMP functions by autocycling strand displacement DNA synthesis at a constant temperature.[11,17−20] The LAMP reaction relies upon production of stem-loop DNA molecules with multiple inverted target repeats. Since LAMP uses a set of four or six different primers targeting different loci of a target gene, allowing the recognition of independent sequences, its specificity in gene amplification is therefore superior to PCR. Additionally, the rapid turnaround and isothermal nature of LAMP make it suitable for point-of-care healthcare settings.

To address the low-throughput nature of conventional NAA methods, microfluidic platforms, especially droplet-based microfluidics,[10,21−27] can be a promising solution to miniaturize the NAA processing. Droplet-based microfluidics can compartmentalize NAA reaction cocktails into ∼10^4−10^6

Received: October 9, 2018
Accepted: March 14, 2019

DOI: 10.1021/acssensors.8b01206
ACS Sens. XXXX, XXX, XXX−XXX

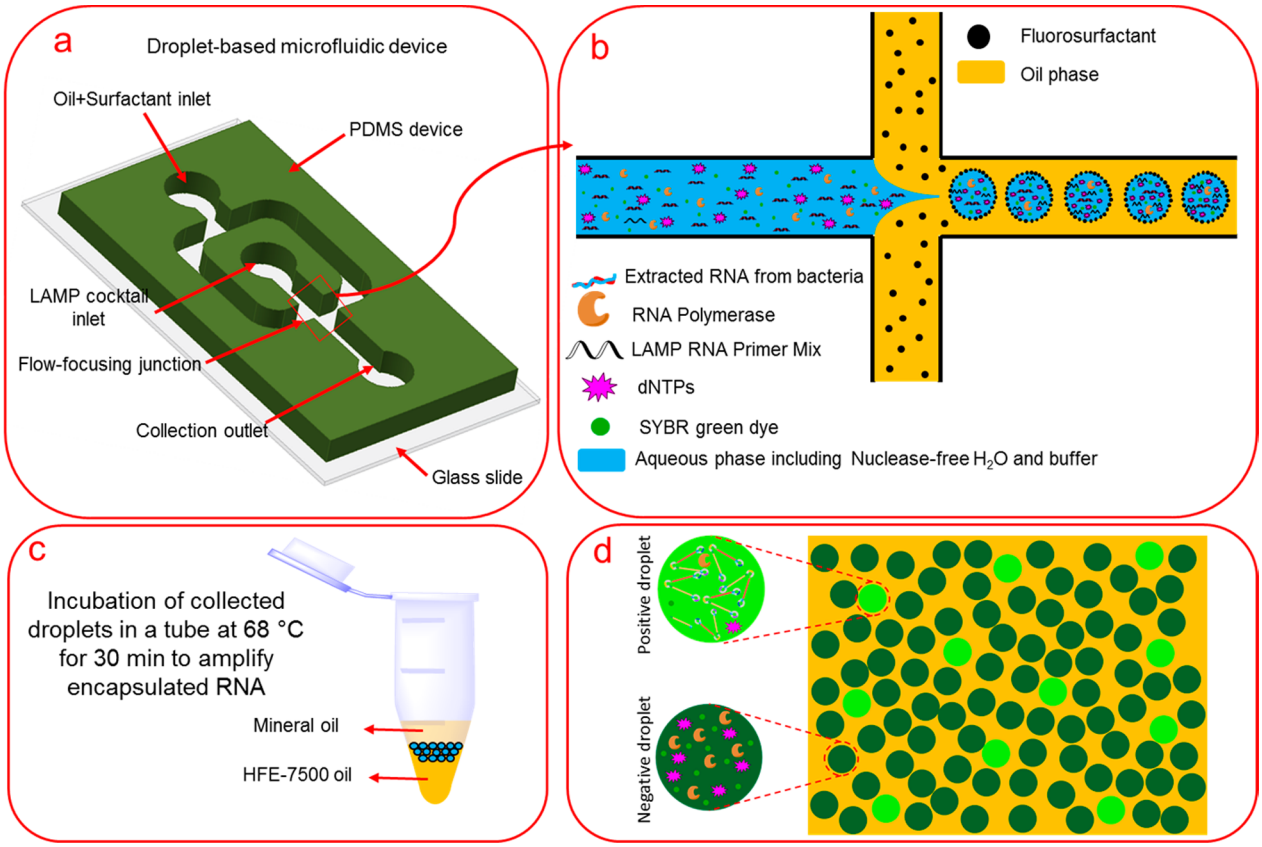

Figure 1. Schematic representations of sample encapsulation, incubation, and screening. (a) The schematic of the microfluidic flow-focusing device for encapsulation of the LAMP reaction cocktail into water-in-oil droplets. (b) Schematic view of the flow-focusing cross-junction. The water-in-oil droplets are collected into a PCR tube. (c) Incubation of collected droplets in a thermocycler at 68 °C for 30 min. (d) Fluorescent imaging and "Yes/No" quantification of the incubated positive droplets.

(depending on droplets' size) water-in-oil microdroplets[28−30] with each functioning as an independent microreactor, making it possible to perform high-throughput NAA in a simple and straightforward manner with short turnaround time, which is particularly important for analyzing biological matrices with a low population density of bacteria.[31−33]

Herein, we bring LAMP and droplet-based microfluidics together in an optimized, operational condition to detect *S. typhimurium* in pure culture and a contaminated milk matrix. The method relies on confining the mixture of the LAMP reaction cocktail and the extracted RNA from targeted bacteria within small water-in-oil microdroplets. As a result, a higher throughput of RNA amplification is expected. We propose a new theoretical model to predict the average number of droplets necessary to screen for the first positive droplet (confirming the sample infection). Then, we use our proposed model to find the detection limits of *S. typhimurium* in pure culture and contaminated milk samples. Extracted RNA templates, instead of DNA, are used to perform LAMP reactions due to a larger number of RNA copies extracted from bacteria lysate than genomic DNA. We also investigate the effect of droplet size (one of the most important process parameters) on detection limits. To examine the LAMP specificity in droplet-based microfluidics, we test the ability to differentiate *S. typhimurium* from two other prevalent bacterial contamination agents in milk: Gram-negative *Shigella flexneri* (*S. flexneri*) and Gram-positive bacteria *Staphylococcus aureus* (*S. aureus*).

EXPERIMENTAL SECTION

Bacteria Culture. All bacterial strains (*S. typhimurium*, *S. flexneri*, and *S. aureus*) were streaked on nutrient agar plates, and a colony of bacteria was incubated in 3 mL of lysogeny broth (LB) medium, as needed, at 37 °C overnight.

RNA Extraction. A 1 mL aliquot (5×10^8 bacteria cells) of the overnight grown culture (~12 h) was centrifuged at 5000*g* for 10 min. The bacterial pellets were collected by removing the supernatant. Then, bacterial cell lysis and RNA extraction and purification were performed according to the protocol provided by the QIAamp RNeasy Mini Kit (50) (QIAGEN, Valencia, CA). The RNA template concentration was measured using a Nanodrop (Nanodrop 1000, Thermo Scientific, MA).

To extract RNA from contaminated milk samples, the milk samples were purposefully contaminated by inoculation of *S. typhimurium*, *S. flexneri*, and *S. aureus* cultures separately into three identical milk samples at a ratio of 1:1 (milk:bacteria culture) for 2 h. After inoculation, the milk was centrifuged to separate the bacterial pellets and prepared for RNA extraction. Because the bacteria culture was diluted by 50% during inoculation in milk, to extract RNA from the bacteria, the volume of bacterial suspension used for extraction was twice that compared to the pure culture sample to compensate for the dilution effect.

Primer Design. On the basis of the *invA* gene (GenBank, accession no. NC_003197) of *S. typhimurium*, the *ipaH* gene (M32063) of *S. flexneri*, and the *nuc* gene (V01281.1) of *S. aureus*, three sets of LAMP primers (Table S1) were designed using PrimerExplorer4 software. The sequences of primers were purchased from Integrated DNA Technologies (IDT) Co., (Coralville, IA).

LAMP Reaction and Gel Electrophoresis. The LAMP assay was conducted as previously described by Notomi et al.[34] The LAMP kit

DOI: 10.1021/acssensors.8b01206
ACS Sens. XXXX, XXX, XXX−XXX

was provided by Lucigen (Madison, WI, USA). Briefly, 25 μL of the reaction cocktail for each experiment contained 2.5 μL of 10X OmniAmp Buffer, 0.8 μL of dNTPs mixture (25 mM each), 0.5 μL of $MgSO_4$ (100 mM), 0.5 μL of betaine (5 M), 1.25 μL of 20X CYBR green dye, 2.5 μL of 10X target-specific primer mix, 0.5 μL of OmniAmp RNA/DNA polymerase, and 1 μL of target RNA. The rest of the reaction cocktail (15.95 μL) contained nuclease-free water. Conventional gel electrophoresis (Sub-Cell GT, Bio-Rad, CA) was used to analyze LAMP amplicons by casting 1.5 wt % agarose in ethylenediaminetetraacetic acid (EDTA) solution. LAMP products were subjected through gel electrophoresis by applying 130 V voltage for 40 min.

Fabrication of the Microfluidic Device, Droplet Generation, and Merging. A standard soft photolithography technique was used to fabricate the flow-focusing microfluidic device for droplet generation.[35,36] The details of fabrication along with a schematic description are provided in Figure S1 of the Supporting Information. After fluorescent imaging of each sample, we used 20% 1*H*,1*H*,2*H*,2*H*-perfluoro-1-octanol (PFO) (Alfa Aesar, MA, USA) solution in HFE-7500 to merge the droplets and extract the LAMP products for gel electrophoresis. A 1:1 (v/v) ratio of PFO solution/droplet carrier solution was used.

Fluorescence Imaging. For fluorescence imaging, a monolayer of droplets was imaged using a ZOE Fluorescent Cell Imager (Bio-Rad, California, USA).

RESULTS AND DISCUSSION

Description of the Microfluidic Platform. Figure 1a depicts a three-dimensional schematic of the microfluidic device, known as a flow-focusing design[29,30] (see Figure S1 for the fabrication process) for water-in-oil droplet generation. A fluorosurfactant (2% w/w) soluble in a fluorinated oil (HFE-7500) and RNA-added LAMP reaction cocktail (see Materials and Methods) served as the continuous and dispersed phases, respectively, and were injected into the microfluidic device using exterior and interior inlets (shown as "oil + surfactant inlet" and "LAMP cocktail inlet," respectively). Due to the high interfacial tension between the water and oil phases, the water phase divides into microdroplets at the intersection (cross-junction) of the channels, as can be seen in Figure 1b. It has been shown that the influence of the surfactant on the LAMP reagents[31,37,38] is negligible because the contact between the biological sample and the fluorosurfactant is minimal. The droplets are collected into a PCR tube, and the mineral oil is added into the tube. The mineral oil covers the droplets due to the lower density, 0.8 g/cm^3, and avoids the water evaporation from droplets during droplet thermal incubation in a thermocycler for 30 min at 68 °C (Figure 1c). The optimization of incubation time, temperature, and reagent concentrations is discussed in the Supporting Information and in Figure S2. In the next step, the droplets are examined using a hemocytometer to determine the end-point "Yes/No (positive/negative)" fluorescence quantification (Figure 1d). Screening for the first positive droplet (in which the LAMP amplification has been successfully performed) is the indicator to determine whether the examined sample is contaminated with any target bacteria.

Mathematical Yes/No Binary Model. Finding the first positive droplet (confirming bacterial contamination of the sample) completes the screening process in a pool of millions of droplets, thereby resulting in a faster biosensor to be used in diagnostics applications. At high RNA concentrations, a high portion of the screened droplets will feature positive, and accordingly, the detection time of the screening process—as an indicator of whether the sample is contaminated or not—is short. In contrast, at low initial RNA concentration, the screening process becomes prolonged as a large number of droplets must be screened to detect the very first positive one ($N_{positive}$). To estimate the average number of droplets required for screening ($\langle N_{positive} \rangle$), we developed a simple theoretical and statistical model.

Intuitively, $\langle N_{positive} \rangle$ is inversely correlated with the RNA concentration in the prepared reaction cocktail. In a highly RNA concentrated reaction cocktail, a small $\langle N_{positive} \rangle$ is expected, whereas for a low concentrated reaction cocktail, $\langle N_{positive} \rangle$ will be large. To calculate the mathematical expectation of $N_{positive}$—i.e., $\langle N_{positive} \rangle$—we used eq 1

$$\langle N_{positive} \rangle = \sum_{i=1}^{N} i p_i \tag{1}$$

where N is the overall number of generated droplets; i is the index of the first droplet identified as positive; and p_i is the likelihood of the i^{th} droplet to be the first positive droplet. For the i^{th} droplet to be the first positive one, all droplets screened before must be negative. Accordingly, a recurrence relation between p_i and p_{i+1} is obtained

$$p_{i+1} = p_i \frac{N - k - i + 1}{N - i} \tag{2}$$

where k is the overall number of positive droplets. The derivation of this recurrence relation is discussed in the Supporting Information. Given the recurrence relation between p_{i+1} and p_i described by eq 2, we computed the average number of droplets required to be screened for a large N, shown in Figure 2 as a function of concentration.

The average number of droplets required to be screened to find the first positive one, for different concentrations—i.e., the number of RNA templates over the number of generated droplets—is depicted in Figure 2a. In addition, Figure 2b shows the likelihood of finding zero, one, or multiple RNA templates in a single droplet for different concentrations which feature a Poisson distribution.[21,37,39] Basically, once the number of RNA templates is by order(s) of magnitude smaller than the number of droplets, the number of droplets found to contain no RNA template dominates, and virtually all the positive droplets include only one copy of RNA, equal to the number of positive droplets (Figure 2b-I and 2b-II). The probability of finding several templates in a single droplet is negligible. As the concentration increases, the number of droplets with several RNA templates becomes significant, and thus, the number of RNA is not equivalent to the number of positive droplets. In fact, as expected, for the large N (in comparison to the number of RNA templates) at low concentrations, $\langle N_{positive} \rangle$ asymptotes to N/k (Figure 2a, 2b-I, and 2b-II). Subsequently, at a given concentration (C), the average index of the first positive droplet is $\sim 1/C$ (for large N compared to the number of RNA). As can be seen in Figure 2a, 2b-III, and 2b-IV, once the total number of RNA templates increases and becomes comparable to the number of droplets, the approximation to $1/C$ fails. Since the time required for screening is crucial solely for the case of a low RNA to droplet ratio, one can find this by simply assuming that $\langle N_{positive} \rangle \sim 1/C$, and at high concentrations, $\langle N_{positive} \rangle \sim 1$, which can be evaluated in a very short period of time.

Detection Limit of *S. typhimurium* in Pure Culture. To measure the detection limit for *S. typhimurium* in pure cultures, RNA was extracted from a sample containing 5×10^8 colony

DOI: 10.1021/acssensors.8b01206
ACS Sens. XXXX, XXX, XXX−XXX

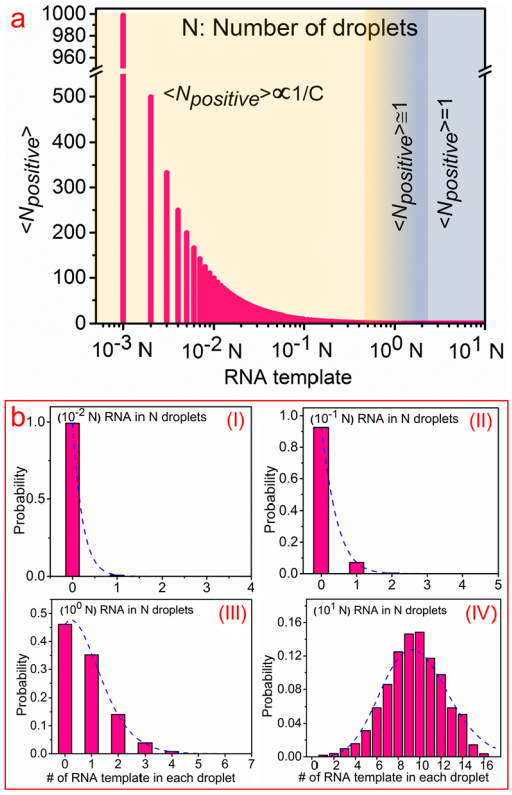

Figure 2. Statistical model and Poisson distribution for finding the first positive droplet and absolute quantification of RNA templates, respectively. (a) Statistical model for prediction of the number of droplets $\langle N_{positive} \rangle$ necessary to be screened for finding the first positive droplet at different initial concentrations of RNA loaded in N number of droplets. As the number of RNA templates is substantially less than the number of droplets, $\langle N_{positive} \rangle \propto \frac{1}{C}$, whereas the number of droplets is identical to number of RNA templates, $\langle N_{positive} \rangle \cong$ or = 1. (b) The Poisson distribution shows the probability that an individual droplet will have zero, one, or more than one RNA template. As the number of RNA templates increases relative to the number of droplets, the probability of having multiple RNA copies in an individual droplet increases accordingly and approaches a normal distribution. The blue dashed plots show the Poisson distribution.

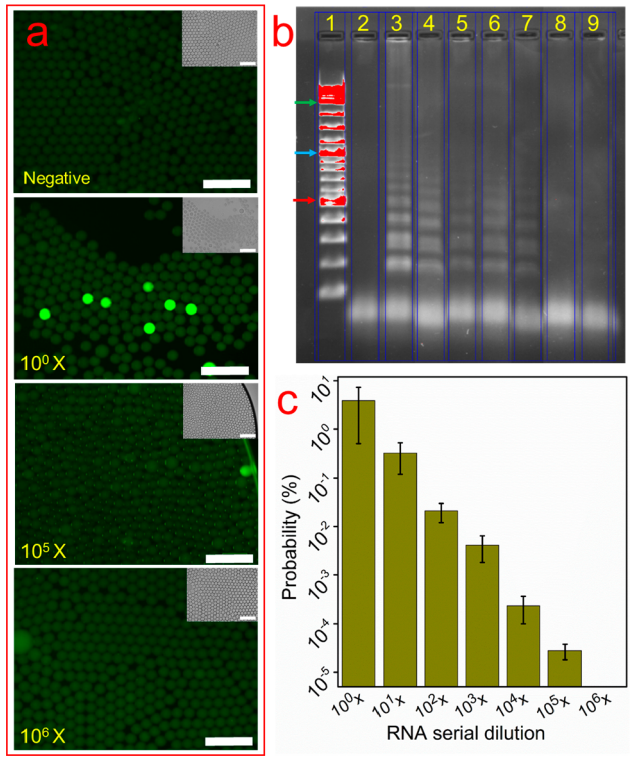

Figure 3. Assessing the detection limits for *S. typhimurium* in pure bacterial culture. (a) Fluorescence images of negative sample and positive samples prepared using the consecutive 10-fold serial dilutions of extracted *S. typhimurium* RNA. The inset figures are bright-field images of the corresponding fluorescent images. (b) Agarose gel electrophoresis results of the extracted amplicons. Lane 1: 2 log DNA ladder, lane 2: negative control (no added RNA in the reaction cocktail), and lanes 3–9: positive samples with consecutive 10-fold serial dilutions (dilution factor 10^0 X, 10^1 X, 10^2 X, 10^3 X, 10^4 X, 10^5 X, and 10^6 X). On the gel image, there are three arrows, shown in red, blue, and green colors, representing 0.5, 1, and 3 Kbp bands, respectively. (c) Probability of finding positive droplets in samples prepared with consecutive 10-fold serial dilutions which drop to essentially zero when the dilution factor is greater than 10^5 X.

forming units (CFUs) eluted in 50 μL of nuclease-free water. With the known starting amount of bacteria, we used 1 μL of the 50 μL in a 25 μL reaction mixture, and this was considered the original concentration (10^0 X). Eight LAMP reaction cocktails were made—one negative control and seven positive samples with different RNA concentrations (dilution factor = 10^0 X, 10^1 X, 10^2 X, 10^3 X, 10^4 X, 10^5 X, and 10^6 X). After encapsulation and incubation of the samples, the droplets were screened, and the fields of view of the 20 μm droplets generated from each of the corresponding reaction cocktails are shown in Figure 3a. The results (Figure 3a) show that the likelihood of finding positive (bright) droplets is lower as the RNA concentration decreases in the prepared reaction cocktails. To test the samples with different concentrations, we screened adequate numbers of droplets according to our proposed model (Figure 2a) to satisfy $\langle N_{positive} \rangle$. Approximately 4% of droplets are positive in samples prepared using original extracted RNA (10^0 X sample) (Figure 3c). According to Poisson distribution discussed in Figure 2b, it can fulfill the "10^{-1} N RNA in N number of droplets" state—there are either none or one RNA template in each droplet (Figure 2b-II).

Then, given ~10^6 generated droplets prepared with an initial 25 μL reaction mixture and the percentage of positive droplets, we performed the absolute quantification of *invA*-RNA templates added to the reaction mixture which would be ~4 × 10^4. Therefore, using the known initial number of *S. typhimurium* used for RNA extraction (5 × 10^8 CFU/mL), eluted in 50 μL of nuclease-free water, we utilized 1 μL of 50 μL RNA solution to prepare a 25 μL LAMP reaction cocktail at the original concentration (dilution factor = 10^0 X) and to identify ~4 × 10^4 copies of the RNA template. We infer the sensitivity to be 1 positive droplet per 250 CFU of *S. typhimurium*. Therefore, the total extracted RNA would be ~2 × 10^6. Moreover, the results (Figure 1a) show that no positive droplets can be seen after five 10-fold serial dilutions of the original extracted RNA. Then, the detection limit of pure *S. typhimurium* should be 5000 CFU/mL in the sample or 25 RNA template/25 μL LAMP reaction cocktail.

After absolute quantification of extracted RNA and determining the detection limit, the amplicons from each reaction were extracted by merging the droplets using PFO and subjected to the agarose gel electrophoresis (Figure 3b). No band, as expected, was obtained for the negative control (i.e., the reaction cocktail without the target RNA template,

DOI: 10.1021/acssensors.8b01206
ACS Sens. XXXX, XXX, XXX−XXX

lane 2 in Figure 3b). In contrast, multiple visible bands are displayed for the positive samples (lanes 3−9 in Figure 3b, corresponding to the different concentrations prepared by 10-fold serial dilutions of the extracted RNA templates). In agreement with Figure 3a, the visible bands obtained from gel electrophoresis become smeared by consecutive 10-fold serial dilutions of the target RNA. We also counted the positive droplets and showed the probability of finding positive droplets for each prepared sample. The probability (Figure 3c) approaches zero by the sample with dilution factor of 10^5 X of the original extracted RNA target (10^0 X), as was qualitatively demonstrated in Figure 3a.

Droplet size may also influence the detection limit of our proposed technique. We used two flow-focusing microfluidic devices, which had 20 and 40 μm sized cross-junctions to produce droplets with the targeted sizes (20 or 40 μm). Distribution of the droplet sizes for the 20 and 40 μm droplet samples is presented in Figure 4a, confirming the majority of the droplets featured the expected sizes (20 and 40 μm). To examine the impact of droplet size on the detection limit, one

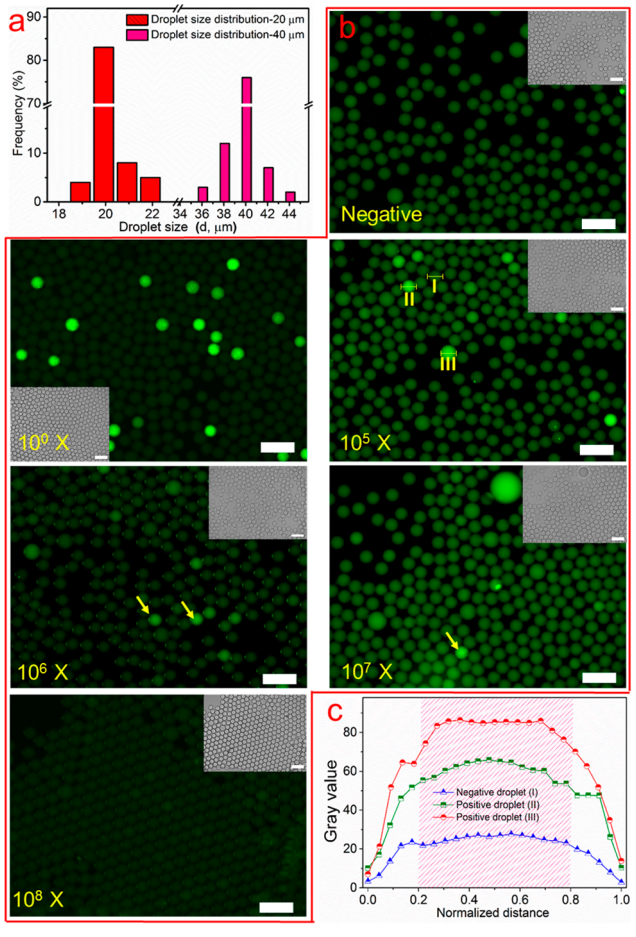

Figure 4. Droplet size effect on detection limit for pure bacterial culture. (a) Droplet size distribution of the generated 20 and 40 μm. (b) Fluorescent images of the 40 μm droplets for the detection of *S. typhimurium* in negative control and positive samples: 10^0 X, 10^7 X, and 10^8 X. The inset figures are bright-field images of the corresponding fluorescent ones. The scale bars are 100 μm. (c) Plot of gray value intensity of droplet fluorescent intensity using ImageJ for positive and negative droplet definition. Gray values of three screened droplets versus 60% of the normalized screening distance of the droplet diameter.

negative control and five positive reaction cocktails with different concentrations of the RNA were prepared as before in 10-fold serial dilutions and then encapsulated in 40 μm droplets. As the estimated detection limit of the *S. typhimurium* sample using the 20 μm droplet system was shown to be at an approximate dilution factor = 10^5 X, as shown in Figure 3, we tested the 40 μm droplet system for the ability to detect *S. typhimurium* at a dilution factor of $\geq 10^5$ X, as well as a negative control (without adding RNA template) and the undiluted (10^0 X) concentration. No positive droplet was observed in the negative control sample ("negative" in Figure 4b). Moreover, Figure 4b represents different fields of view of the 40 μm droplets incorporating reaction cocktails with different amounts of RNA, confirming the detection of the bacteria within the sample up to a dilution factor of 10^7 X. This demonstrates the improvement of the detection limit using 40 μm droplet systems by 2 orders of magnitude better than that of the 20 μm droplets. The main reason for the detection limit improvement is that the initial reaction cocktail features the same number of RNA templates but is encapsulated in a smaller number of droplets. Consequently, the probability of finding positive droplets in the same concentration of added RNA template in the reaction cocktail is greater for 40 μm droplets compared to the 20 μm ones. However, the weak contrast between positive and negative signals in the droplets after 30 min incubation makes the positive droplets harder to detect. Therefore, either longer incubation time is required for the 40 μm droplets to obtain an acceptable light intensity comparable to that obtained for the 20 μm droplets or the decision making between positive/negative droplets needs to be improved based on their current fluorescent intensities. To address the issue, we developed a mathematical model to facilitate positive/negative decision making. We quantitatively adjust the positive or negative statues of the droplet using a light-intensity-based criterion, in which the emitted fluorescent light from the droplets was converted to gray values using ImageJ. The average gray values within a 0.6 normalized middle distance of the droplets' diameter were measured. The droplets displaying average light intensities greater than twice the negative control were considered positive. For instance, the gray value obtained along the diameters for three selected droplets, as shown in Figure 4b (10^5 X), are measured and plotted in Figure 4c. The average gray value within the normal diameter of the negative droplet was ~25, while the two others were measured as ~59 and ~86, respectively. Therefore, these two droplets are identified as positive. Moreover, a comparison between the detection limits and detection time of our data and several other platforms which have been used for pathogenic bacteria detection is provided in Table S2. The functionality and efficiency of a biosensor can be evaluated as both detection limit and detection time.

Detection Limit of *S. typhimurium*-Contaminated Milk Samples. We also tested the functionality of this technique for milk samples inoculated with *S. typhimurium* The concentration of RNA extracted from the *S. typhimurium* pure and milk-contaminated cultures (measured using a nanodrop instrument) is shown in Figure 5a. As shown in this figure, the concentration of extracted RNA from the milk sample is significantly lower than the pure culture. The fluorescent images of droplets generated for *S. typhimurium*-contaminated milk samples are shown in Figure 5b, demonstrating the technique was able to positively identify bacteria up to the sample with dilution factor of 10^3 X. Our results show that the

DOI: 10.1021/acssensors.8b01206
ACS Sens. XXXX, XXX, XXX−XXX

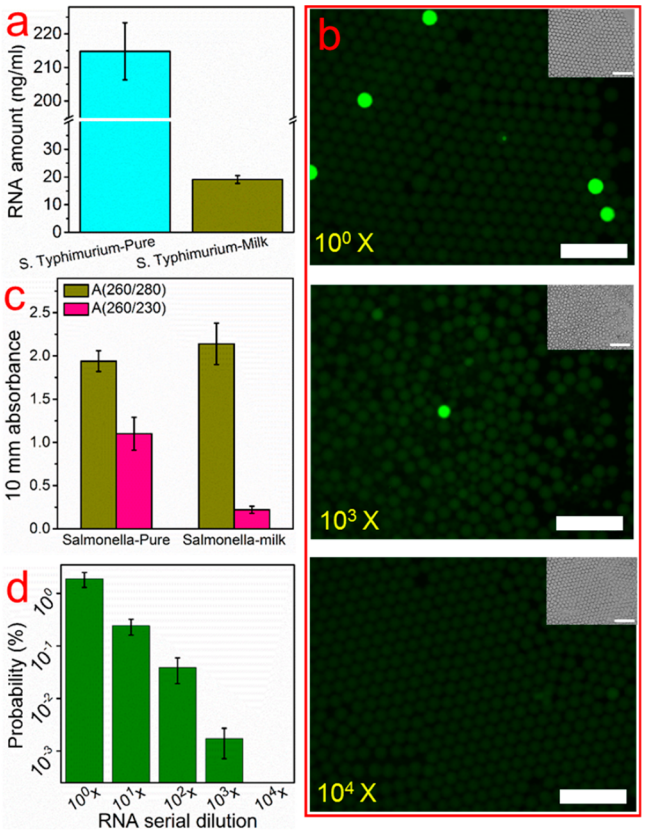

Figure 5. Functionality of the sensor for bacteria-contaminated milk sample. (a) The amount of RNA extracted from inoculated *S. typhimurium* in both pure and contaminated milk samples. (b) Fluorescence images of 20 μm droplets, testing the LAMP reaction containing RNA extracted from the *S. typhimurium*-contaminated milk sample with different consecutive 10-fold serial dilutions: dilution factor 10^0 X, 10^3 X, and 10^4 X. The inset figures are bright-field images of the corresponding fluorescent ones. (c) $A(260/230)$ and $A(260/280)$ ratios of RNA extracted from *S. typhimurium* in both pure culture and contaminated milk samples. (d) The probability of finding positive droplets in samples prepared by extracting RNA from *S. typhimurium*-contaminated milk in consecutive 10-fold serial dilutions.

overall detection limit for *S. typhimurium* bacteria in contaminated milk is 2 orders of magnitude lower than pure culture (pure culture detection limit was a dilution factor of 10^5 X *S. typhimurium* shown in Figure 3a). Given the initial concentration of bacteria inoculated in the milk sample (5×10^8 CFU/mL), the detection limit is measured around 5×10^5 CFU/mL of bacteria in the milk sample. Moreover, similar to a pure culture, we perform the absolute quantification of RNA templates extracted from bacteria inoculated in the milk sample.

To find the reason for the poorer detection limit for the contaminated milk compared to the pure bacterial culture samples, we used a Nanodrop machine to measure the ultraviolet (UV) absorbance at wavelengths 230, 260, and 280 nm. Nucleic acids (DNA and RNA) and proteins have maximum absorbance at 260 and 280 nm, respectively, while a strong absorbance at 230 nm may indicate the peptides of the cell wall and membrane or the presence of impurities such as organic compounds and chaotropic salts, which can disrupt hydrogen bonding between molecules.[40] The $A(260/230)$ and $A(260/280)$ ratios obtained from both pure and milk-contaminated culture samples are demonstrated in Figure 5c, which showed that $A(260/280)$ is close to or larger than 2, meaning the purification of RNA from genomic DNA was well carried out in both the pure culture and contaminated milk samples. However, the $A(260/230)$ ratio is lower in the contaminated milk samples compared to the pure cultures indicating poorer clearance of impurities in the milk samples. Therefore, NAA inhibitors and impurities, such as proteins, enzymes, minerals, and fats from milk, can potentially interfere with the LAMP reaction and may be a reason for the poorer detection limit in contaminated milk than the pure culture samples.[41] Moreover, we examined the probability of finding positive droplets of *S. typhimurium* in milk-contaminated sample (Figure 5d). Our results show that the probability of finding positive droplets overall was lower for contaminated milk samples than the pure cultures, as shown in Figure 3d.

Specificity of LAMP-Assisted Droplet-Based Microfluidics Sensor. Primer specificity has profound impacts on detection performance and efficacy. To demonstrate the specificity of the designed primers targeting the *invA* gene of *S. typhimurium*, we chose two other bacterial sources of milk contamination: *S. flexneri* (Gram-negative) and *S. aureus* (Gram-positive). We prepared three different reaction cocktails, separately adding primers targeting the *invA* gene of *S. typhimurium* to RNA extracted from *S. typhimurium* (positive sample), *S. flexneri* (negative control), and *S. aureus* (negative control). The reaction cocktails were encapsulated in 20 μm droplets and incubated at 68 °C for 30 min. As shown in Figure 6a-I, we observed positive droplets in the "*invA* targeted primers of *S. typhimurium*/*S. typhimurium* RNA" sample, while there were no positive droplets seen in "*S. typhimurium* primers/*S. flexneri* RNA" and "*S. typhimurium* primers/*S. aureus* RNA" (Figure 6a-II and 6a-III, respectively). Thus, the

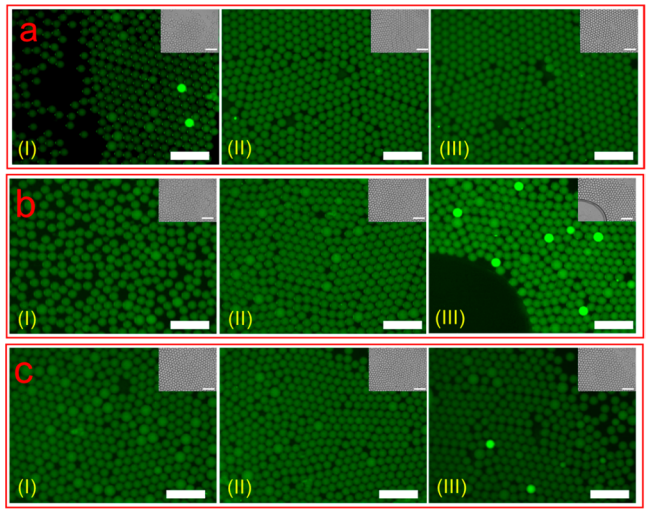

Figure 6. Specificity of the LAMP-assisted droplet-based microfluidics sensor for detecting the targeted bacteria. (a) Fluorescence images of droplets containing: (I) *S. typhimurium* primers/*S. typhimurium* RNA (positive), (II) *S. typhimurium* primers/*S. flexneri* RNA (negative), and (III) *S. typhimurium* primers/*S. aureus* RNA (negative). (b) Fluorescence images of droplets containing: (I) *S. flexneri* primers/no RNA template (negative), (II) *S. flexneri* primers/*S. typhimurium* RNA (negative), and (III) *S. flexneri* primers/*S. flexneri* RNA (positive). (c) Fluorescence images of droplets containing: (I) *S. aureus* primers/no RNA template (negative), (II) *S. aureus* primers/*S. typhimurium* RNA (negative), and (III) *S. aureus* primers/*S. aureus* RNA (positive). The scale bars are 100 μm.

DOI: 10.1021/acssensors.8b01206
ACS Sens. XXXX, XXX, XXX−XXX

results demonstrate the remarkable specificity of the designed LAMP primers for the *invA* gene of *S. typhimurium* which do not cross-react with the RNA of the closely related *S. flexneri*.

Conversely, using two other sets of primers (listed in Table S1), targeting the *ipaH* and *nuc* genes of *S. flexneri* and *S. aureus*, respectively, two other sets of reaction cocktails were prepared to study the specificity of the LAMP reaction in our droplet-based microfluidic system. Each reaction cocktail includes a positive and two negative controls. Either the *ipaH*- or *nuc*-designed primers were separately added to i: no RNA (negative controls—Figure 6b-I and 6c-I, respectively), ii: extracted *S. typhimurium* RNA (negative controls—Figure 6b-II and 6c-II, respectively), and iii: extracted *S. flexneri* or *S. aureus* RNAs, respectively (positive samples—Figure 6b-III and 6b-III, respectively). The trends were similar for both *ipaH*- and *nuc*-reaction sets, in which there were some positive droplets observed in the positive samples (Figure 6b-III and 6c-III) and no positive droplets observed in the negative controls (Figure 6b-I, 6b-II, 6c-I, and 6c-II). Therefore, the results (Figure 6) demonstrate that the LAMP-assisted droplet-based microfluidic technique is specific for the bacteria detection and generally NAA.

CONCLUSIONS

In conclusion, we showed that loop-mediated isothermal amplification and droplet-based microfluidics together can introduce a rapid and high-throughput method for nucleic acid amplification, specifically focusing on detection of pathogenic bacteria in this study. Millions of water-in-oil droplets incorporating the cocktail of LAMP reagents were rapidly generated via a flow-focusing microfluidic device and incubated at an isothermal condition (68 °C) for 30 min. Initially, we proposed a mathematical Yes/No binary model to determine the average number of droplets required for screening to find the first positive droplet, which can speed-up the turnaround time. Using our mathematical model, we showed that the 20 μm droplets worked up to 10^5 X and 10^3 X dilutions (detection limits) of the original extracted RNA sample from the pure *S. typhimurium* culture and contaminated milk samples. We also found that the detection limit of this platform is improved with increasing droplet size, although longer incubation time or proposing a robust mathematical light-intensity-based criterion model was needed to obtain proper fluorescent contrast between negative and positive droplets. We also showed how specific this platform is working for detecting a target bacteria with no false positives. Bringing these features together could open an avenue to overcome the limitation of some other NAA methods by eliminating the need for temperature cycling, being high-throughput, and being very applicable for detection of pathogenic bacteria/viruses in food, agricultural, and clinical healthcare settings.

ASSOCIATED CONTENT

Supporting Information

The Supporting Information is available free of charge on the ACS Publications website at DOI: 10.1021/acssensors.8b01206.

The LAMP reaction optimization, the primer sequences, the soft lithography steps to make the flow-focusing device, and Table S2 containing the comparison between detection limits and detection time (PDF)

AUTHOR INFORMATION

Corresponding Author

*Tel.: +1 (607) 255-2923. E-mail: alireza@cornell.edu.

ORCID

Alireza Abbaspourrad: 0000-0001-5617-9220

Notes

The authors declare no competing financial interest.

ACKNOWLEDGMENTS

The authors gratefully acknowledge the Cornell Nanoscale Science and Technology Facility, which is supported through the NSF NNCI program (Grant Number ECCS31542081). The authors would also like to thank Prof. Martin Wiedmann, Dr. Rachel Miller, Dr. Shelly Clark, Dr. Yichang Liu, and Anna Sophia Harrand for their great help and invaluable scientific guidance during this project.

REFERENCES

(1) Chun, H. J.; Kim, S.; Han, Y. D.; Kim, K. R.; Kim, J.-H.; Yoon, H.; Yoon, H. C. Salmonella Typhimurium Sensing Strategy Based on the Loop-Mediated Isothermal Amplification Using Retroreflective Janus Particle as a Nonspectroscopic Signaling Probe. *ACS Sensors* **2018**, *3* (11), 2261−2268.

(2) Pajoumshariati, S. R.; Azizi, M.; Zhang, S.; Dogan, B.; Simpson, K. W.; Abbaspourrad, A. A Microfluidic-Based Model for Spatially Constrained Culture of Intestinal Microbiota. *Adv. Funct. Mater.* **2018**, *28* (48), 1805568.

(3) Shirzaei Sani, E.; Portillo-Lara, R.; Spencer, A.; Yu, W.; Geilich, B. M.; Noshadi, I.; Webster, T. J.; Annabi, N. Engineering Adhesive and Antimicrobial Hyaluronic Acid/Elastin-like Polypeptide Hybrid Hydrogels for Tissue Engineering Applications. *ACS Biomater. Sci. Eng.* **2018**, *4* (7), 2528−2540.

(4) Annabi, N.; Rana, D.; Shirzaei Sani, E.; Portillo-Lara, R.; Gifford, J. L.; Fares, M. M.; Mithieux, S. M.; Weiss, A. S. Engineering a sprayable and elastic hydrogel adhesive with antimicrobial properties for wound healing. *Biomaterials* **2017**, *139*, 229−243.

(5) Azizi, M.; Zaferani, M.; Dogan, B.; Zhang, S.; Simpson, K. W.; Abbaspourrad, A. Nanoliter-Sized Microchamber/Microarray Microfluidic Platform for Antibiotic Susceptibility Testing. *Anal. Chem.* **2018**, *90* (24), 14137−14144.

(6) Park, S. H.; Aydin, M.; Khatiwara, A.; Dolan, M. C.; Gilmore, D. F.; Bouldin, J. L.; Ahn, S.; Ricke, S. C. Current and emerging technologies for rapid detection and characterization of Salmonella in poultry and poultry products. *Food Microbiol.* **2014**, *38*, 250−262.

(7) Tennant, S. M.; Toema, D.; Qamar, F.; Iqbal, N.; Boyd, M. A.; Marshall, J. M.; Blackwelder, W. C.; Wu, Y.; Quadri, F.; Khan, A.; Aziz, F.; Ahmad, K.; Kalam, A.; Asif, E.; Qureshi, S.; Khan, E.; Zaidi, A. K.; Levine, M. M. Detection of Typhoidal and Paratyphoidal Salmonella in Blood by Real-time Polymerase Chain Reaction. *Clin. Infect. Dis.* **2015**, *61*, S241−S250.

(8) Yang, Q.; Wang, F.; Jones, K. L.; Meng, J.; Prinyawiwatkul, W.; Ge, B. Evaluation of loop-mediated isothermal amplification for the rapid, reliable, and robust detection of Salmonella in produce. *Food Microbiol.* **2015**, *46*, 485−493.

(9) Cui, Y.; Liu, F.; Li, X.; Wang, L.; Wang, H.; Chen, G.; Yuan, L.; Brash, J. L.; Chen, H. Improvement in the Thermal Stability of Pyrophosphatase by Conjugation to Poly(N-isopropylacrylamide): Application to the Polymerase Chain Reaction. *ACS Appl. Mater. Interfaces* **2015**, *7* (39), 21913−21918.

(10) Eastburn, D. J.; Sciambi, A.; Abate, A. R. Ultrahigh-Throughput Mammalian Single-Cell Reverse-Transcriptase Polymerase Chain Reaction in Microfluidic Drops. *Anal. Chem.* **2013**, *85* (16), 8016−8021.

(11) Safavieh, M.; Kanakasabapathy, M. K.; Tarlan, F.; Ahmed, M. U.; Zourob, M.; Asghar, W.; Shafiee, H. Emerging Loop-Mediated Isothermal Amplification-Based Microchip and Microdevice Tech-

DOI: 10.1021/acssensors.8b01206
ACS Sens. XXXX, XXX, XXX−XXX

nologies for Nucleic Acid Detection. *ACS Biomater. Sci. Eng.* **2016**, *2* (3), 278−294.
(12) Dean, F. B.; Hosono, S.; Fang, L.; Wu, X.; Faruqi, A. F.; Bray-Ward, P.; Sun, Z.; Zong, Q.; Du, Y.; Du, J.; Driscoll, M.; Song, W.; Kingsmore, S. F.; Egholm, M.; Lasken, R. S. Comprehensive human genome amplification using multiple displacement amplification. *Proc. Natl. Acad. Sci. U. S. A.* **2002**, *99* (8), 5261−5266.
(13) Vincent, M.; Xu, Y.; Kong, H. Helicase-dependent isothermal DNA amplification. *EMBO Rep.* **2004**, *5* (8), 795−800.
(14) Van Ness, J.; Van Ness, L. K.; Galas, D. J. Isothermal reactions for the amplification of oligonucleotides. *Proc. Natl. Acad. Sci. U. S. A.* **2003**, *100* (8), 4504−4509.
(15) Lin, X.; Huang, X.; Urmann, K.; Xie, X.; Hoffmann, M. R. Digital Loop-Mediated Isothermal Amplification on a Commercial Membrane. *ACS Sensors* **2019**, *4* (1), 242−249.
(16) Notomi, T.; Masubuchi, H.; Okayama, H.; Amino, N.; Hase, T.; Yonekawa, T.; Watanabe, K. Loop-mediated isothermal amplification of DNA. *Nucleic Acids Res.* **2000**, *28* (12), e63−e63.
(17) Qin, A.; Fu, L. T.; Wong, J. K. F.; Chau, L. Y.; Yip, S. P.; Lee, T. M. H. Precipitation of PEG/Carboxyl-Modified Gold Nanoparticles with Magnesium Pyrophosphate: A New Platform for Real-Time Monitoring of Loop-Mediated Isothermal Amplification. *ACS Appl. Mater. Interfaces* **2017**, *9* (12), 10472−10480.
(18) Li, F.; Liu, X.; Zhao, B.; Yan, J.; Li, Q.; Aldalbahi, A.; Shi, J.; Song, S.; Fan, C.; Wang, L. Graphene Nanoprobes for Real-Time Monitoring of Isothermal Nucleic Acid Amplification. *ACS Appl. Mater. Interfaces* **2017**, *9* (18), 15245−15253.
(19) Kong, J. E.; Wei, Q.; Tseng, D.; Zhang, J.; Pan, E.; Lewinski, M.; Garner, O. B.; Ozcan, A.; Di Carlo, D. Highly Stable and Sensitive Nucleic Acid Amplification and Cell-Phone-Based Readout. *ACS Nano* **2017**, *11* (3), 2934−2943.
(20) Martin, A.; Grant, K. B.; Stressmann, F.; Ghigo, J.-M.; Marchal, D.; Limoges, B. Ultimate Single-Copy DNA Detection Using Real-Time Electrochemical LAMP. *ACS Sensors* **2016**, *1* (7), 904−912.
(21) Mashaghi, S.; Abbaspourrad, A.; Weitz, D. A.; van Oijen, A. M. Droplet microfluidics: A tool for biology, chemistry and nanotechnology. *TrAC, Trends Anal. Chem.* **2016**, *82*, 118−125.
(22) Xie, X.; Zhang, W.; Abbaspourrad, A.; Ahn, J.; Bader, A.; Bose, S.; Vegas, A.; Lin, J.; Tao, J.; Hang, T.; Lee, H.; Iverson, N.; Bisker, G.; Li, L.; Strano, M. S.; Weitz, D. A.; Anderson, D. G. Microfluidic Fabrication of Colloidal Nanomaterials-Encapsulated Microcapsules for Biomolecular Sensing. *Nano Lett.* **2017**, *17* (3), 2015−2020.
(23) Choi, C.-H.; Lee, H.; Abbaspourrad, A.; Kim, J. H.; et al. Triple Emulsion Drops with An Ultrathin Water Layer: High Encapsulation Efficiency and Enhanced Cargo Retention in Microcapsules. *Adv. Mater.* **2016**, *28* (17), 3340−3344.
(24) Ortiz, R.; Chen, J. L.; Stuckey, D. C.; Steele, T. W. J. Poly(methyl methacrylate) Surface Modification for Surfactant-Free Real-Time Toxicity Assay on Droplet Microfluidic Platform. *ACS Appl. Mater. Interfaces* **2017**, *9* (15), 13801−13811.
(25) Knudsen, S. M.; von Muhlen, M. G.; Schauer, D. B.; Manalis, S. R. Determination of Bacterial Antibiotic Resistance Based on Osmotic Shock Response. *Anal. Chem.* **2009**, *81* (16), 7087−7090.
(26) Jiang, X.; Jing, W.; Sun, X.; Liu, Q.; Yang, C.; Liu, S.; Qin, K.; Sui, G. High-Throughput Microfluidic Device for LAMP Analysis of Airborne Bacteria. *ACS Sensors* **2016**, *1* (7), 958−962.
(27) Xu, P.; Zheng, X.; Tao, Y.; Du, W. Cross-Interface Emulsification for Generating Size-Tunable Droplets. *Anal. Chem.* **2016**, *88* (6), 3171−3177.
(28) Scheler, O.; Kaminski, T. S.; Ruszczak, A.; Garstecki, P. Dodecylresorufin (C12R) Outperforms Resorufin in Microdroplet Bacterial Assays. *ACS Appl. Mater. Interfaces* **2016**, *8* (18), 11318−11325.
(29) Abbaspourrad, A.; Zhang, H.; Tao, Y.; Cui, N.; Asahara, H.; Zhou, Y.; Yue, D.; Koehler, S. A.; Ung, L. W.; Heyman, J.; Ren, Y.; Ziblat, R.; Chong, S.; Weitz, D. A. Label-free single-cell protein quantification using a drop-based mix-and-read system. *Sci. Rep.* **2015**, *5*, 12756.
(30) Cui, N.; Zhang, H.; Schneider, N.; Tao, Y.; Asahara, H.; Sun, Z.; Cai, Y.; Koehler, S. A.; de Greef, T. F. A.; Abbaspourrad, A.; Weitz, D. A.; Chong, S. A mix-and-read drop-based in vitro two-hybrid method for screening high-affinity peptide binders. *Sci. Rep.* **2016**, *6*, 22575.
(31) Pajoumshariati, S. R.; Azizi, M.; Wesner, D.; Miller, P. G.; Shuler, M. L.; Abbaspourrad, A. Microfluidic-Based Cell-Embedded Microgels Using Nonfluorinated Oil as a Model for the Gastrointestinal Niche. *ACS Appl. Mater. Interfaces* **2018**, *10* (11), 9235−9246.
(32) Rotem, A.; Ram, O.; Shoresh, N.; Sperling, R. A.; Goren, A.; Weitz, D. A.; Bernstein, B. E. Single-cell ChIP-seq reveals cell subpopulations defined by chromatin state. *Nat. Biotechnol.* **2015**, *33*, 1165.
(33) Sidore, A. M.; Lan, F.; Lim, S. W.; Abate, A. R. Enhanced sequencing coverage with digital droplet multiple displacement amplification. *Nucleic Acids Res.* **2016**, *44* (7), e66−e66.
(34) Notomi, T.; Mori, Y.; Tomita, N.; Kanda, H. Loop-mediated isothermal amplification (LAMP): principle, features, and future prospects. *J. Microbiol.* **2015**, *53* (1), 1−5.
(35) Duffy, D. C.; McDonald, J. C.; Schueller, O. J. A.; Whitesides, G. M. Rapid Prototyping of Microfluidic Systems in Poly(dimethylsiloxane). *Anal. Chem.* **1998**, *70* (23), 4974−4984.
(36) Zaferani, M.; Cheong, S. H.; Abbaspourrad, A. Rheotaxis-based separation of sperm with progressive motility using a microfluidic corral system. *Proc. Natl. Acad. Sci. U. S. A.* **2018**, *115* (33), 8272−8277.
(37) Mao, A. S.; Shin, J.-W.; Utech, S.; Wang, H.; Uzun, O.; Li, W.; Cooper, M.; Hu, Y.; Zhang, L.; Weitz, D. A.; Mooney, D. J. Deterministic encapsulation of single cells in thin tunable microgels for niche modelling and therapeutic delivery. *Nat. Mater.* **2017**, *16*, 236.
(38) Utech, S.; Prodanovic, R.; Mao, A. S.; Ostafe, R.; Mooney, D. J.; Weitz, D. A. Microfluidic Generation of Monodisperse, Structurally Homogeneous Alginate Microgels for Cell Encapsulation and 3D Cell Culture. *Adv. Healthcare Mater.* **2015**, *4* (11), 1628−1633.
(39) Clausell-Tormos, J.; Lieber, D.; Baret, J.-C.; El-Harrak, A.; Miller, O. J.; Frenz, L.; Blouwolff, J.; Humphry, K. J.; Köster, S.; Duan, H.; Holtze, C.; Weitz, D. A.; Griffiths, A. D.; Merten, C. A. Droplet-Based Microfluidic Platforms for the Encapsulation and Screening of Mammalian Cells and Multicellular Organisms. *Chem. Biol.* **2008**, *15* (5), 427−437.
(40) Schmid, F.-X. Biological Macromolecules: UV-visible Spectrophotometry. In *eLS*.
(41) Hu, Y.; Xu, P.; Luo, J.; He, H.; Du, W. Absolute Quantification of H5-Subtype Avian Influenza Viruses Using Droplet Digital Loop-Mediated Isothermal Amplification. *Anal. Chem.* **2017**, *89* (1), 745−750.

DOI: 10.1021/acssensors.8b01206
ACS Sens. XXXX, XXX, XXX−XXX